Tellus (1993), 45B, 160–178
Printed in Belgium – all rights reserved

TELLUS
ISSN 0280–6509

A 3-D global simulation of the advective transport of passive tracers from various northern hemisphere sources

By KOJI YAMAZAKI and MASARU CHIBA, *Climate Research Department, Meteorological Research Institute, 1–1 Nagamine, Tsukuba, Ibaraki 305, Japan*

(Manuscript received 27 August 1991; in final form 3 July 1992)

ABSTRACT

Two-year transport simulations are performed for passive tracers continuously emitted from Japan, Europe, North America and Amazon regions in order to study transport processes of anthropogenic gases such as CO_2 and halocarbons. Three-dimensional wind data produced by the Meteorological Research Institute global spectral model with rhomboidal 24 truncation and 23 levels are used. Globally, there are three regions within which the transport of tracer is relatively rapid. These are the tropics, and the northern/southern extratropics. Within the tropics, the Pacific and Indian Ocean regions may be considered as further subdivisions. Transports between regions are much slower. In the case of a Japanese source, an equatorward transport occurs mainly in the lower troposphere during winter associated with the Asian winter monsoon circulation. The tracers are advected upward over the equatorial Indian Ocean and transported into the southern hemisphere. A significant seasonal oscillation in tracer density develops in the Antarctic region with the maximum in early June. In the cases of European and North American sources, an equatorward transport is slow and a poleward transport is enhanced in winter. In all cases, transport to the southern extratropics occurs in the upper troposphere because of upward advection in the tropical region. The tracer density increases with altitude in the troposphere in the southern extratropics except over Antarctica. Over Antarctica, the tracer density decreases with altitude and the horizontal distribution is rather uniform at the surface, indicating downward transport of low-density stratospheric air.

1. Introduction

Atmospheric General Circulation Models (AGCM) have been used not only for climate simulations but also for simulations of chemical tracer transport. A transport simulation of passive tracer released in the midlatitude lower stratosphere was made by Mahlman and Moxim (1978) using the 11-layer Geophysical Fluid Dynamics Laboratory (GFDL) model about one decade ago. Early applications of AGCMs to tracer transport were mainly aimed at simulating the distribution of ozone, e.g., Schlesinger and Mintz (1979) at University of California, Los Angeles (UCLA) and Mahlman et al. (1980). Ozone plays an important role in middle atmosphere dynamics and this was the motivation of above studies.

Recently, AGCMs have been widely used for simulating transports of many chemical tracers such as CO_2, chlorofluorocarbons (CFCs) and fluorocarbons. Applications to CO_2 were made by Fung et al. (1983, 1987) and Tans et al. (1990), and to fluorocarbons by Prather et al. (1987), using the model of the Goddard Institute for Space Studies (GISS). These gases have a strong greenhouse effect and are increasing due to human activity.

As a first step to investigate the global transport of anthropogenic gases using the Meteorological Research Institute (MRI) global spectral model, this paper presents the results of a global, long-term simulation of passive and conservative tracers. "Passive" means that the tracers move with the air and do not affect the atmospheric circulation. "Conservative" means that there are no sources and sinks within the atmosphere and no chemical reactions are considered. Tracers are emitted from three regions in the northern hemisphere and the Amazon region. The three regions are Japan, Europe and North America. These regions are selected to mimic the release of anthropogenic gases by industrial activities. The Amazon region is selected to mimic the release of CO_2 or carbon by biomass burning. Our aim is to clarify the role of the large-scale circulation and the location of sources in determining the global distribution of anthropogenic gases, in particular to show how tracers are transported from source regions to remote regions such as the southern hemisphere or Antarctica. A focus is placed upon describing long-term mean distributions and temporal variations of tracers.

2. Model and experiments

2.1. Model

The Meteorological Research Institute global spectral model (MRI-GSPM: Chiba et al., 1986) is used in this study. The model is based on the primitive equations formulated in $\sigma(p/p_s)$ coordinates. It has 23 levels and its uppermost level is at about 0.05 hPa ($\sim$70 km). The vertical grid spacing is $2\sim3$ km below 1.5 hPa and $6\sim7$ km above. In the horizontal, the model uses the spectral transform method with a rhomboidal 24 truncation (R24). The associated Gaussian grid has 80 points in longitude with a spacing of 4.5° and 62 points in latitude with an approximate spacing of 2.95°.

Physical processes such as radiation, large-scale condensation, cumulus convection, planetary boundary layer processes, and ground hydrology are parameterized. The effect of gravity wave drag is simply parameterized by Rayleigh friction. The longwave radiation scheme is based on the multi-parameter random model of Shibata and Aoki (1989), and Shibata (1989). The solar radiation scheme of Lacis and Hansen (1974) is slightly modified to include calculations of partial cloudiness. The diurnal cycle of solar radiation is explicitly calculated as well as the seasonal cycle. The sea surface temperatures are prescribed based on 15-year mean monthly climatology made by Climate Analysis Center/NOAA. The details of the model and the climatology of R13L23 version are found in Shibata and Chiba (1990a) and the performance of the model of R24L11 version over the Antarctic region is given in Shibata and Chiba (1990b).

The model was integrated for about 4 years starting from the initial conditions on 1 November 1984. The simulated winds, temperature and surface pressure fields were stored every 2 h on magnetic tape from the model's June 1986. These 2-hourly data were used for the transport calculation of passive tracers. Yamazaki and Chiba (1992) made a similar transport simulation with 12-hourly data for 10-month period starting from the model's December 1984. They discussed short-term transport as well as long-term transport. Main results in Yamazaki and Chiba (1992) are similar to those in the present study.

The MRI-GSPM reproduces most features of the

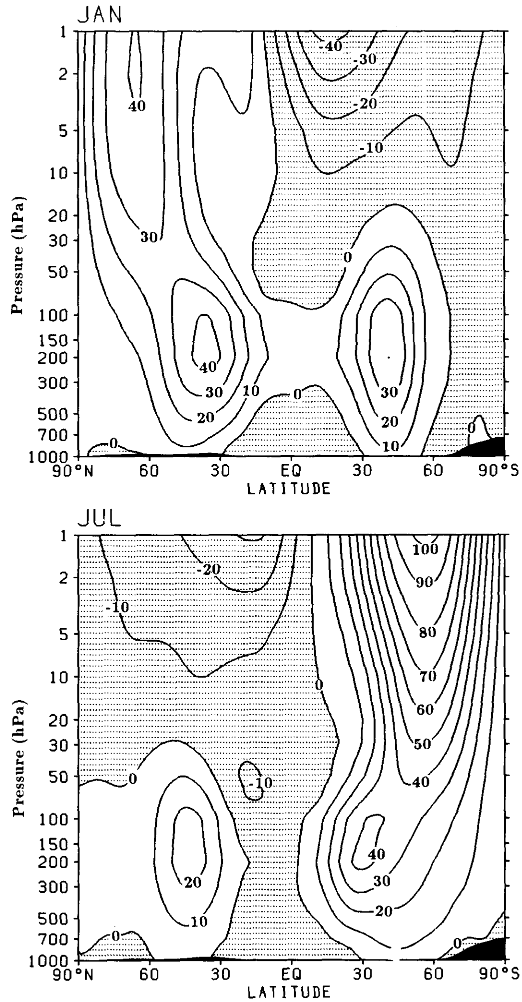

Fig. 1. Two-year-mean zonal-mean zonal wind from the MRI-GSPM for January and July. Contour interval is 10 m/s. Negative values (easterlies) are stippled.

large-scale general circulation well. The simulated zonal mean zonal wind and mass stream function are shown in Figs. 1 and 2, respectively. In the Northern Hemisphere, the subtropical westerly jet is located near 40° N, 200 hPa and the peak is about 40 m/s in January and 25 m/s in July (Fig. 1). The magnitude and position of the jet approximately accord with the observation, though the simulated position is shifted poleward especially in January. In the Southern Hemisphere, the subtropical jet is located near 45° S, 200 hPa and its magnitude is about 40 m/s in January.

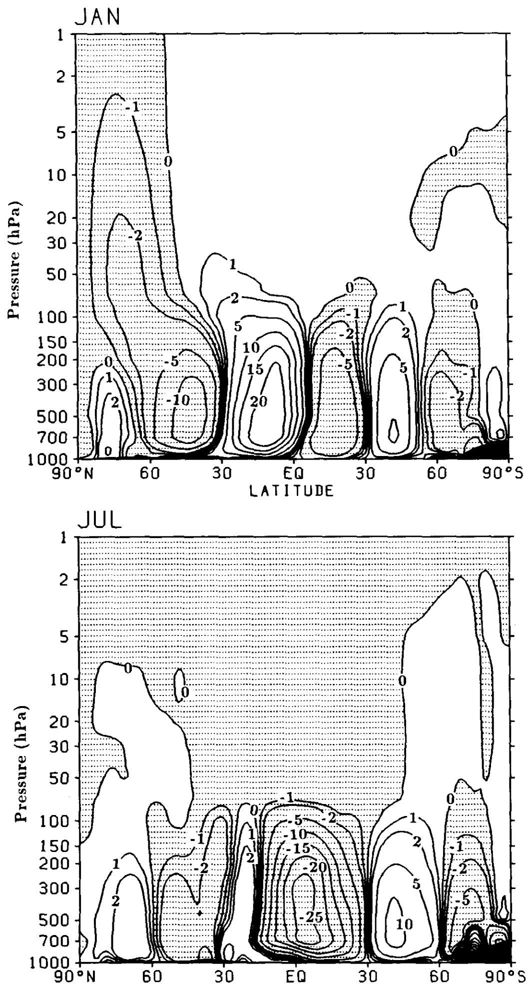

Fig. 2. Two year mean zonal mean mass stream function ($\times 10^{10}$ kg/s) from the MRI-GSPM. Stippling indicates negative values (clockwise circulation).

It shifts to 30° S and strengthens slightly in July. The magnitude is slightly overestimated in both months. In July, observations show the high-latitude ($\sim 50°$ S) jet in the mid- and lower-troposphere. The model does not simulate this double-jet feature well, though the westerly speed increases in high latitudes in July. In the stratosphere, the seasonal variation of zonal wind is well simulated and the wind speed approximately accords with the observations.

The zonal mean mass stream function produced by the model is shown in Fig. 2 for January and July. In the troposphere, the three-cell structure, i.e., the Hadley cell, Ferrel cell, and Polar cell, is reasonably well simulated in both months. The strength of the Hadley cell is slightly stronger than observation. The Ferrel cell is about the same magnitude as observation except for an overestimation in the northern winter. The centers of the cells are located at about 700 hPa level, which accords with the observations well. In the stratosphere, the stream function is reasonably well simulated in both hemispheres and months. Note that the stream functions shown in Fig. 2 are the Eulerian mean circulations and not equal to the transport circulations (WMO, 1985 and references therein). Also note that the model atmosphere undergoes a significant interannual variation as in the real atmosphere and the 2 year means are shown in Figs. 1 and 2.

The stationary and transient waves are the dominant meridional atmospheric transport mechanism outside the low latitudes. Therefore, the accuracy of these components should be addressed in addition to the zonally-averaged fields. The stationary and total (stationary + transient) eddy components of the meridional wind field are defined as follows;

$$V_S^2 \equiv [(\bar{V} - [\bar{V}])^2], \tag{1}$$

$$V_T^2 \equiv [(V - [\bar{V}])^2], \tag{2}$$

where the overbar denotes the monthly mean and the square bracket denotes the zonal mean. The simulated values are shown in Fig. 3 and the corresponding observations based on the 10-year (1981–90) NMC data are shown in Fig. 4. In the observed data, the wind above 50 hPa is a non-linear balance wind calculated from the geopotential height and the wind in the low latitudes is

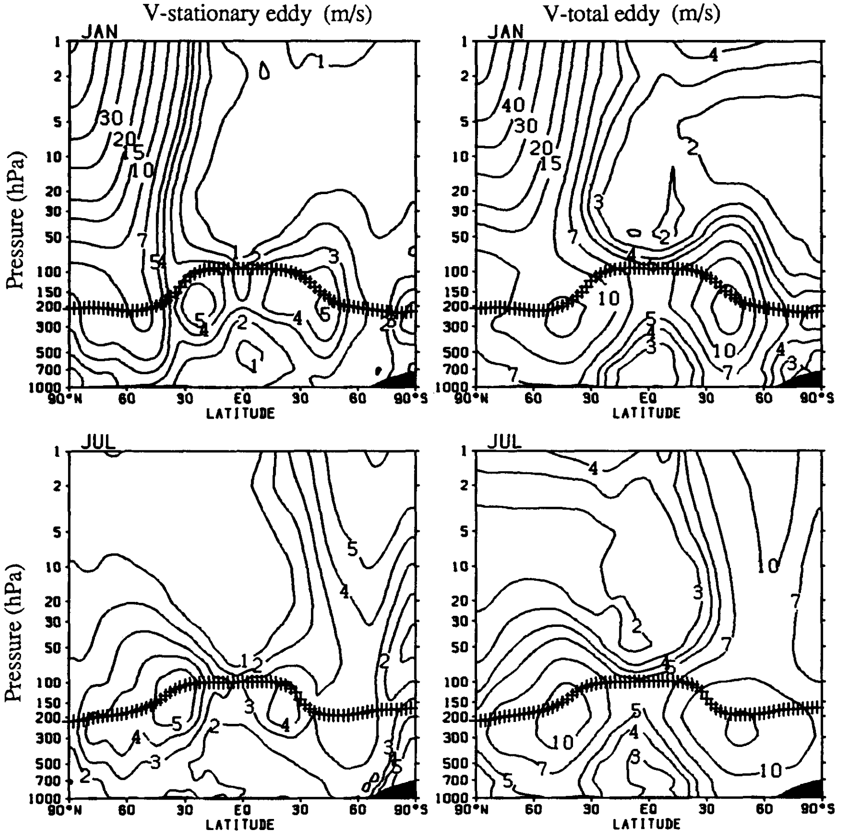

Fig. 3. Simulated stationary (left) and total (stationary + transient) (right) components of the meridional wind for January (top) and July (bottom). See eqs. (1) and (2) in the text for the definitions. Contours are 1, 2, 3, 4, 5, 6, 7, 10, 15, 20, 30, 40, 50 m/s. Crosses denote the tropopause height.

linearly interpolated from winds in the middle latitudes. Also the tropopause height defined as the height where temperature rapse rate is less than 0.2 K km^{-1} is shown in Figs. 3 and 4.

In January, the stationary component of the meridional wind (V_S) has two peaks in the northern troposphere. One peak is situated equatorward of the subtropical jet and its magnitude is about 6 m/s. The other is in the middle latitudes and its magnitude is about 7 m/s. It is connected to the polar stratospheric peak. In the Southern Hemisphere, there are three peaks in the upper troposphere and these magnitudes are 4–5 m/s. The total eddy component of the meridional wind (V_T) in the troposphere shows one peak in each hemisphere at 40–50°N/S. Transient baroclinic waves contribute to these peaks. In the northern stratosphere, a large V_T is found in the north polar upper stratosphere to which stationary waves are the dominant contribution. The simulated eddy components accord with the observations quite well both January and July, except for the overestimate in the northern stratosphere in January.

In summary, the GCM simulates the large-scale features of atmospheric flows with considerable realism.

2.2. *Tracer model*

Tracer model predicts a tracer density using the following three-dimensional transport equation:

$$\frac{\partial \chi}{\partial t} = -\boldsymbol{V} \cdot \nabla_\sigma \chi - \dot{\sigma} \frac{\partial \chi}{\partial \sigma} + \frac{\partial}{\partial \sigma}\left(K_\sigma \frac{\partial \chi}{\partial \sigma}\right) + \text{source}, \tag{3}$$

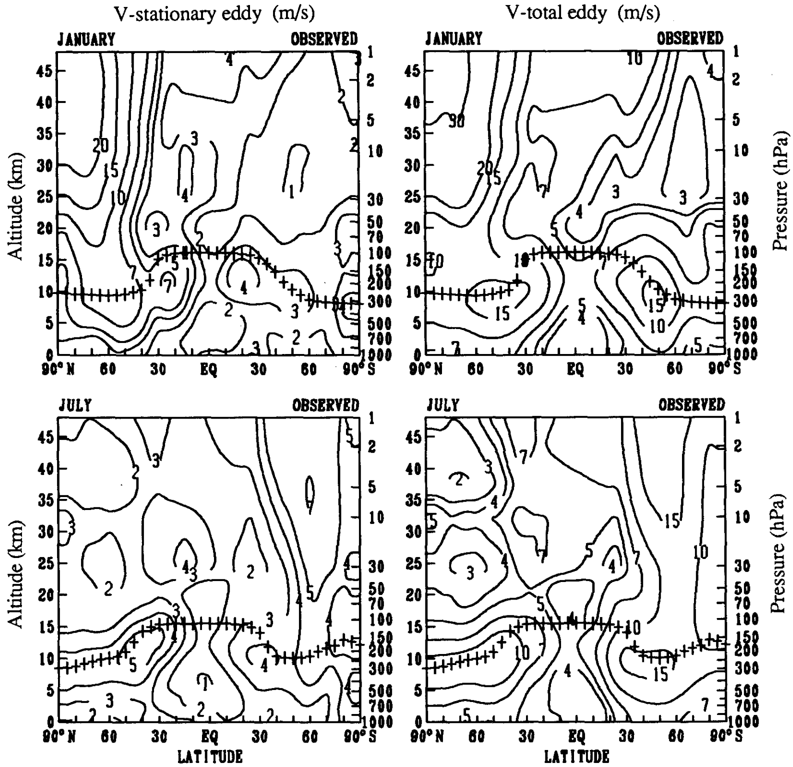

Fig. 4. Same as in Fig. 3 except for observed data.

where χ is tracer density, ∇_σ is the gradient operator on a σ-surface, V is the velocity on a σ-surface, t is time, $\dot{\sigma}$ is the vertical velocity in σ coordinates, K_σ is the vertical diffusion coefficient, and "source" is a source term, which will be described in the Subsection 2.3. Vertical diffusion depends on the stability of the atmosphere and the scheme is based on Louis (1979), which is also used in the MRI-GSPM. The vertical diffusion scheme is applied below level 17 ($\sim$225 hPa). No diffusion is computed above that level for computational efficiency. The one-month test run including vertical diffusion for all levels did not produce discernible differences. In this study, no subgrid-scale horizontal diffusion is included.

It is likely that convection pays a central role in the vertical redistribution of tracers, particularly in the tropics, and so a parameterization of the effect of convection on tracer transport should be included. However, in the present experiment the effect of convection is omitted partly due to the uncertainty of the parameterization and in order to keep experiments clean. The redistribution of tracers due to convection probably occurs on a time scale of an hour, while that due to grid-scale motion occurs on a time scale of a day in the tropics. These time scales are shorter than the large-scale transport time scale. Therefore, the omission of the effect of explicit convection may not cause serious errors in the simulation.

A three-dimensional semi-Lagrangian scheme (for the two-dimensional scheme, see Williamson and Rasch, 1989 and references therein) is used for calculations of advection (1st and 2nd terms of the r.h.s. of eq. (3)). Two-hourly simulated wind data are linearly interpolated to hourly data, and the scheme is applied to these hourly data. The semi-Lagrangian scheme calculates the tracer density at a certain grid point as follows. The point where the air was located one time-step earlier is calculated, and the density at that backward point is obtained by spacewise interpolation. The density at the grid

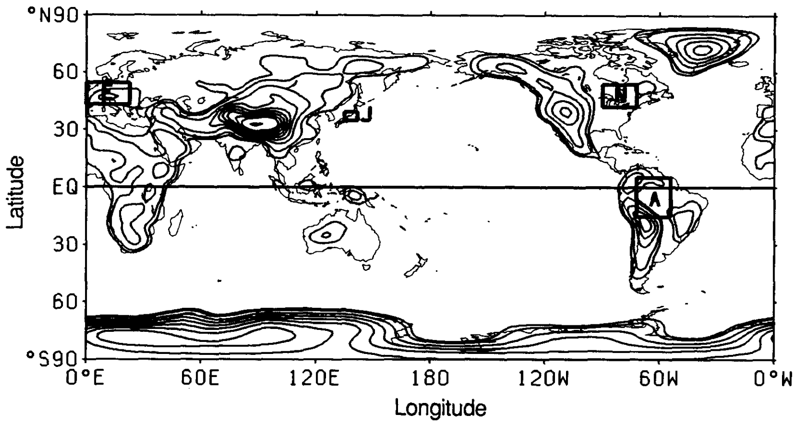

Fig. 5. Topography used in the MRI-GCM-R24 and source regions for transport simulations. Unit of topography is 100 m. Thick rectangles denote source regions. **J** stands for the Japanese source case, **E** stands for the European case, **N** stands for the North American case, and **A** stands for the Amazonian case.

point is set equal to that at the backward point. The scheme works well even when large density gradients exist, and there is no limitation on time step to prevent numerical instabilities. The scheme also preserves the tracer distribution shape well. On the other hand, the scheme does not guarantee conservation of total tracer mass. Therefore, in our calculation a mass correction is made at each time step to preserve total tracer mass, though a preliminary calculation without the correction did not produce significant differences in the tracer distribution pattern.

2.3. Experiments

In this study, a continuous source of tracer gas is placed over a certain region. Experiments are done for four source regions, i.e., Japan, Europe, North America, and Amazon regions as shown in Fig. 5. All the experiments were conducted with zero initial tracer density. At each source grid points, one unit of tracer is emitted per day into the lowest model layer throughout the experiment. The depth of the lowest model layer is about 20 hPa. Since surface pressure varies with time, the emission rate is not exactly constant but almost constant. Therefore, in each experiment the global mean tracer density increases almost linearly with time. Other sources or sinks are not considered. The starting time of the transport calculation is 00 UTC 7 June of the model's year 1986. The calculations were continued for 2 years.

3. Mean distributions

3.1. Japanese source

The horizontal tracer distributions averaged over the last year of the calculation are shown in Fig. 6 for Japanese source. The top panel of Fig. 6 shows the density at the lowest model layer (the surface layer). A maximum in density is found over the source region. The dense region extends eastnortheastward from Japan to the north Pacific. The dense region also extends southwestward to the Indian Ocean. The eastward spread of tracer mainly occurs in summer and the southward spread in winter (Yamazaki and Chiba, 1992). In winter, tracer is transported equatorward by the low-level anticyclonic flow, since Japan is located southeastside of the Siberian high. Some tracer is transported eastward when low pressure systems pass over Japan. In summer, tracer is mostly transported eastward to the north Pacific, since Japan is situated on the westside of the north Pacific subtropical high. The tracer tends to stagnate over the north Pacific region. Near the equator, especially over the Indian Ocean, a steep meridional gradient in tracer density is generated.

At 500 hPa level (middle panel of Fig. 6), a maximum is found over the equatorial Indian Ocean. This large density is generated during winter when tracers are transported from Japan into the Indian Ocean region and they are lifted by upward motion along the Inter Tropical Con-

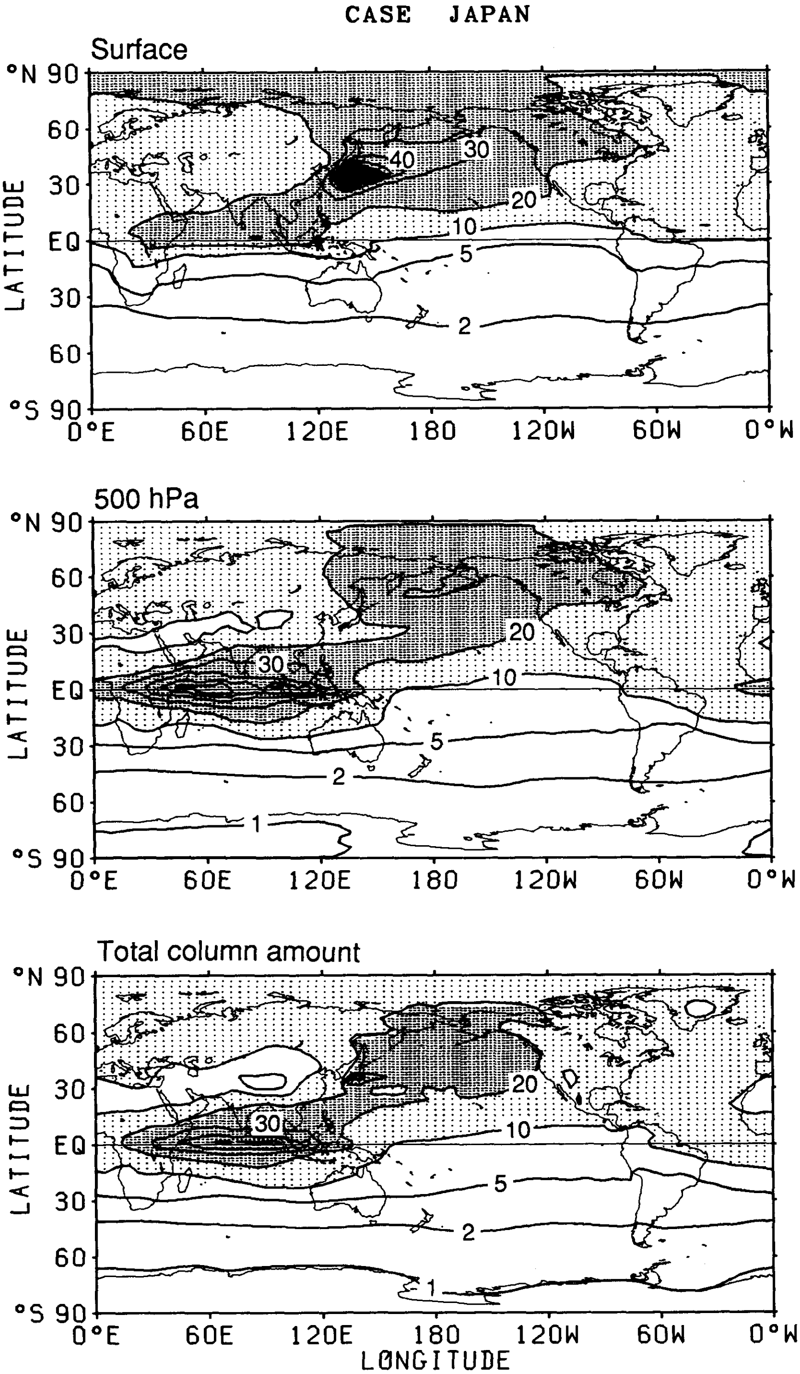

Fig. 6. Horizontal distributions of tracer in the Japanese source case averaged over the last year. Unit is arbitrary. top) at the surface, middle) at 500 hPa, bottom) total column amount. Contour interval is 10 and Contours of 5, 2, 1 are also drawn.

vergence Zone (ITCZ). Some tracer spreads into the Southern Hemisphere from the Indian Ocean region. In the southern extratropics, the distribution is nearly zonally uniform. Another local maximum is found over the north Pacific region, which is generated in summer as mentioned before. In this case, it is clear that the transport is largely affected by the Asian monsoon circulation. It is interesting that no maximum is found over the source region at 500 hPa level.

The bottom panel of Fig. 6 shows the total column amount of tracer, i.e., the vertical integral of tracer density from top to the surface. The low values over the Tibetan plateau, Greenland and the Rockies are partly due to the small air mass over elevated mountains. The pattern is similar to that of density at 500 hPa except for large values over the source region.

The latitude-height section of zonal mean tracer density for the last year is shown in Fig. 7. The contours are drawn with a logarithmic scale. Two maxima are found; one near the source at the surface and the other at the equator in the middle troposphere. The density in the northern extratropical troposphere is rather uniform. This is caused by strong eddies in the northern extratropics (Fig. 3). Around 30° N, low density values intrude from above, because there is a downward motion advecting a tracer-poor stratospheric air into the troposphere. In the tropics, the tracer density is large because tracers tend to be trapped in the tropics due to weak eddy activity. In the Southern Hemisphere, the density decreases toward south. In particular, the meridional gradient in the tracer density is large at 20–30° S. The density in the extratropical troposphere in the

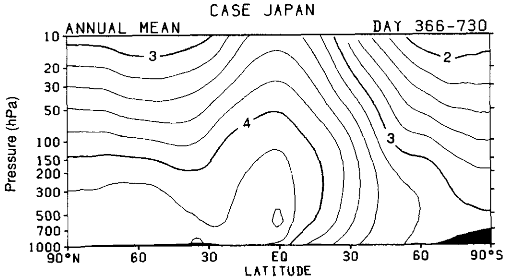

Fig. 7. Zonal mean tracer density averaged over the last one year for the Japanese source case. Unit is arbitrary. Contours are drawn with a logarithmic scale. Contour interval is 0.2.

Southern Hemisphere is about one order smaller than that in the Northern Hemisphere. From the transport point of view, the troposphere seems to be divided into three regions, i.e., the northern extratropics, the tropics and the southern extratropics. It is noteworthy that the density increases with altitude in the southern hemisphere troposphere. This is because tracer from the Northern Hemisphere is lifted near the equator (upward branch of the Hadley cell), and transported into the Southern Hemisphere through the upper troposphere.

At the upper troposphere, the maximum in the meridional distribution occurs near the equator, and is also caused by the Hadley circulation. A similar meridional distribution is observed for CO_2 (Nakazawa et al., 1991a). There is also an upward bulge centered at the equator in the upper troposphere and stratosphere. In the stratosphere the density rapidly decreases with altitude.

3.2. *European source*

The horizontal tracer distributions averaged over the last year of integration are shown in Fig. 8 for a European source. Values are adjusted so that the total source intensity is equal to that for Japanese source by taking into account of the difference in area of the source regions. The other two cases were also adjusted to be able to compare cases.

Patterns for surface, 500 hPa, and total column amount in Fig. 8 are not much different from each other. A maximum in tracer density is found near the source region and the dense region extends eastward. The dense region also extends to the north polar region. Tracer is transported mainly within high latitudes and the poleward transport is enhanced in winter. A steep meridional gradient in tracer density is formed near 40° N especially at the middle troposphere. Transport from the Northern Hemisphere to the Southern Hemisphere is slow compared with the Japanese source case.

The latitude-height section of zonal mean tracer density for the last year is shown in Fig. 9. The density in the high-latitude troposphere is large and relatively uniform. The density decreases toward south in the troposphere. In the middle troposphere, meridional density gradients are large around 30° N and 30° S. In the lower troposphere, contours converge on the equator reflecting the low-level convergent motion of the

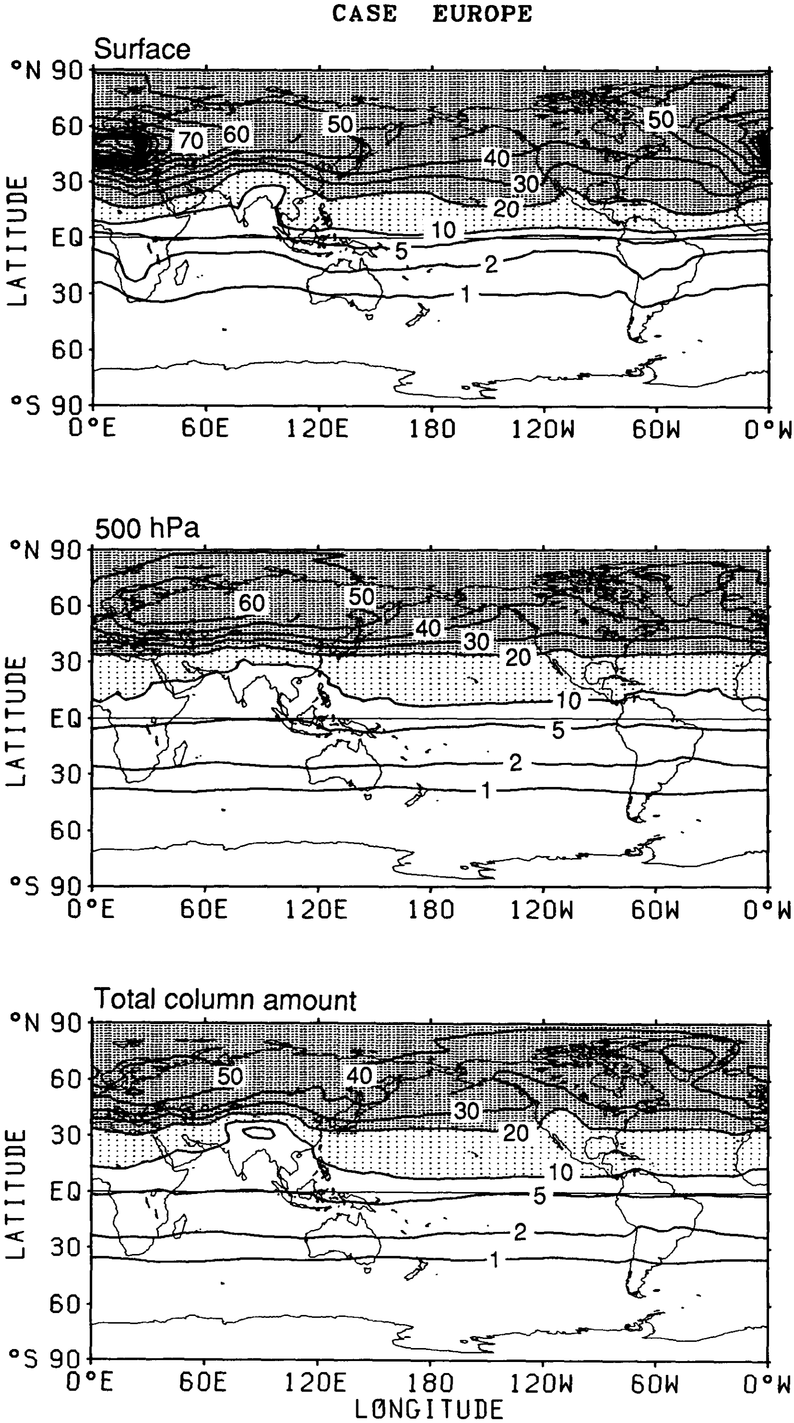

Fig. 8. Same as in Fig. 6 except for the European source case.

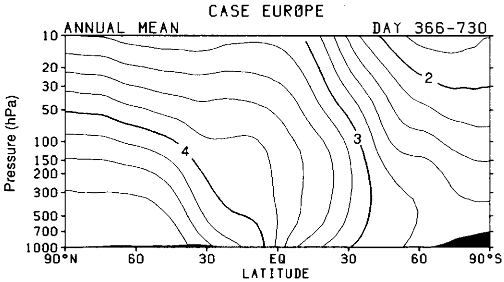

Fig. 9. Same as in Fig. 7 except for the European source case.

Hadley cell. In the southern troposphere the density increases with altitude as in the Japanese source case.

A slight upward buldge is found near the equator in the upper troposphere and the stratosphere. In the stratosphere, the density decreases with altitude in both hemispheres. The density increases poleward in the northern stratosphere. This is probably due to upward transport from the troposphere by eddy activity.

3.3. North American source

This case is similar to the European case. Only the horizontal distribution of total column amount for the last year is shown in Fig. 10. A dense region is generated over north America, the Atlantic Ocean and the north polar region. Both this case and the European case show enhanced transport into the Arctic haze region (Heintzenberg, 1989). In the real Arctic haze, there is a greater contribution from sources in Europe and Russia than those in the north America (Barrie et al., 1989). In our experiment, the north American source region is located at the same latitude as the European region, whereas the actual north American source region is further south. This is probably the main reason for the discrepancy. The European and North American examples also suggest that when a source is located in high latitudes, the tracer transport to the northern subtropical latitudes is slow.

The latitude-height section of zonal mean tracer density for the last year is shown in Fig. 11 for the North American source. This case is almost same as the European case except for a slight difference in the near-surface northern high latitudes. This strongly suggests that a long-term transport from northern high latitudes to somewhere else does not depend significantly upon the location of the source. By comparing this case with the Japanese case, it is noted that the patterns in the Southern Hemisphere are almost same, though the magnitudes are different. This also suggests that a long-term transport pattern from the northern extratropics to the Southern Hemisphere does not depend upon the location of the source, though the speed of transport depends.

Note that above comparisons are based on the

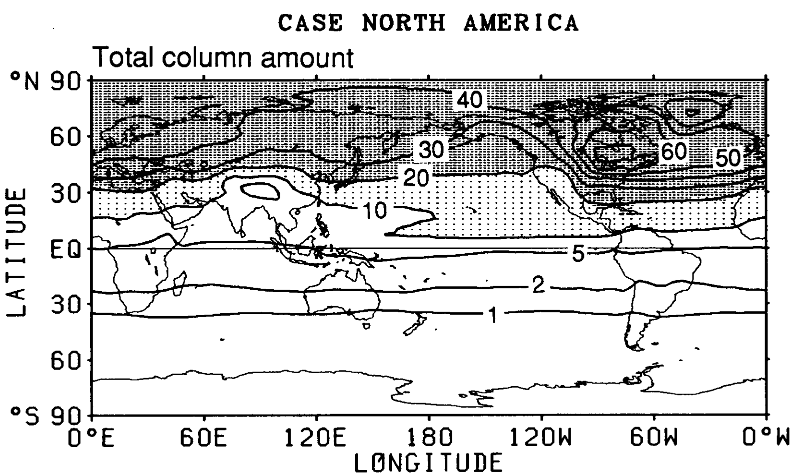

Fig. 10. Same as in Fig. 6 except for the North American source case. Only the figure for total column amount is shown.

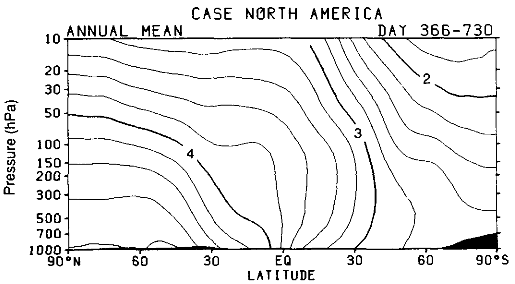

Fig. 11. Same as in Fig. 7 except for the North American source case.

zonal mean quantities. However as shown in the Figs. 6, 8 and 10, the horizontal distribution is nearly zonally uniform in the southern extratropics. Therefore the above comparisons are also valid for the horizontal distribution in the southern extratropics.

3.4. *Amazonian source*

The horizontal tracer distributions averaged over the last year of integration are shown in Fig. 12 for an Amazonian source. At the surface, the maximum is located over the Amazon basin and a very thin dense region extends westward along the equator due to the easterly trade wind. Tracer reaches as far as 160° W, 10° S and then moves upward, because the South Pacific Convergence Zone (SPCZ) is situated there. Therefore, a maximum is found near 160° W, 10° S at 500 hPa level. Over the eastern and central Pacific, the flow is weak westerly in the upper troposphere. Thus tracer returns eastwards towards the eastern Pacific where downward motion is dominant. The tropical Walker circulation, which has the ascending branch over the western Pacific and the descending branch over the eastern Pacific, acts to trap tracer within the cell over the tropical Pacific. The confinement within the Walker cell becomes weak during the austral summer when a strong convection center is located over Brazil. During the austral summer, some tracer is lifted upward, advected southward and spreads to the southern extratropics. Some of the tracers is still advected westward and trapped within the Walker cell.

Transport to the Antarctic region is much faster than in the other cases, because the source is located in the equatorial region. Also, transport into the southern extratropics is enhanced during the austral summer as mentioned before.

The maximum of the zonal mean tracer density is found in the middle troposphere near 10° S (Fig. 13). The pattern is nearly symmetric about 10° S. Near the surface, the density increases with altitude in both hemispheres because transport from the equatorial region to the extratropics mainly takes place through poleward advection in the upper troposphere.

It is interesting that the maximum in the zonal mean appears in the middle troposphere even though the source is at the surface. In the source region, the maximum appears at the lowest layer (see Fig. 12). However, outside the source region, the density has a maximum at the middle troposphere. In the zonal mean, the contribution from outside the source region overcomes that from the source region.

3.5. *Transport to the Antarctic region*

In this subsection, the tracer distribution in the Antarctic region is examined and the cause of the distribution is discussed. Fig. 14 shows the tracer distributions averaged over the last year of integration for the Antarctic region at the surface and at 500 hPa in the Japanese source example. Since other cases are similar to this case in their patterns, only the Japanese source example is discussed. Over the Southern Ocean, the density decreases poleward at both levels. The density at 500 hPa is higher than that at the surface and the peak is located at about 400 hPa (see also Fig. 7). This is because tracers are transported into the Southern Hemisphere through the upper troposphere as mentioned in Subsection 3.1.

Over Antarctica, the density at the surface becomes rather flat, while at 500 hPa it decreases going towards the center of the Antarctic continent. The density decreases with altitude and the maximum is found near the surface. This vertical profile is opposite to that over the Southern Ocean. This strongly suggests that low-density upper-level air i.e., stratospheric air is transported downward there. The air entered into the PBL from above and spreads over Antarctica as the Katabatic winds from the top of the East Antarctic ice sheet flow toward the coast (Shibata and Chiba, 1990b), so causing the uniform tracer distribution over Antarctica at the surface.

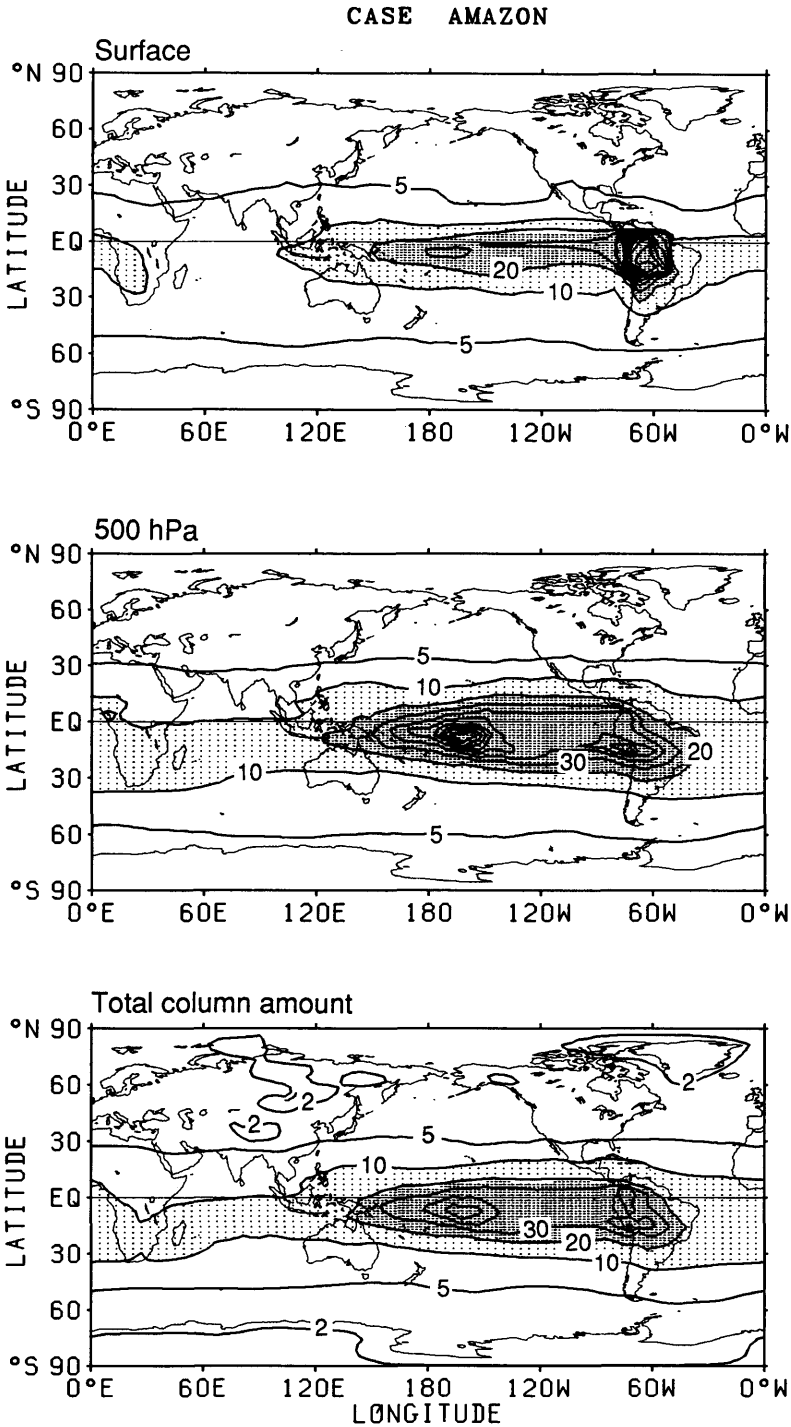

Fig. 12. Same as in Fig. 6 except for the Amazonian source case.

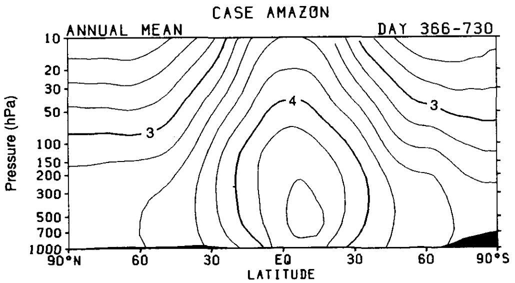

Fig. 13. Same as in Fig. 7 except for the Amazonian source case.

4. Temporal variation

Fig. 15 shows the time-latitude plot of zonal mean tracer density at 500 hPa for the Japanese source example. The figure is plotted using 5-day mean data (pentad data). At the beginning, tracer spreads northwards and southwards from the source latitude. During fall through winter, tracer spreads southwards into the Southern Hemisphere, while the density in the northern extratropics stays rather constant. A maximum is formed near the equator during winter through spring. In early spring, the direction of tracer transport changes from equatorward to northward. During spring through summer, the density in the northern extratropics increases, while that in the southern hemisphere decreases slightly. Again in early fall, the tracer transport changes in direction. The interhemispheric transport clearly shows an annual oscillation.

The pattern for the total column amount is similar to Fig. 15. At the surface, the temporal behavior is similar to Fig. 15 except that a maximum continuously exists near the source latitude. The contour line of 10 in Fig. 15, which is located in the northern extratropics in July of the first year, reaches Antarctica in March of the next year. It took 1 year and 8 months to propagate from the northern source latitude to Antarctica.

Fig. 16 is the same as in Fig. 15 except for the European source example. The interhemispheric transport is slow in this case. It does not show a significant seasonal variation, though the southward progression is enhanced during summer in low-latitudes. The contour line of 10 does not reach Antarctica within the simulation period. Case North America is similar to case Europe and the figure is not shown. In both cases, transport to the Arctic region is enhanced during winter to spring, which is related to the Arctic haze.

Fig. 17 shows the Amazonian source example. The latitude of maximum density migrates between 0° N in summer–fall and 10° S in winter–spring. The contour of 10 reaches Antarctica in

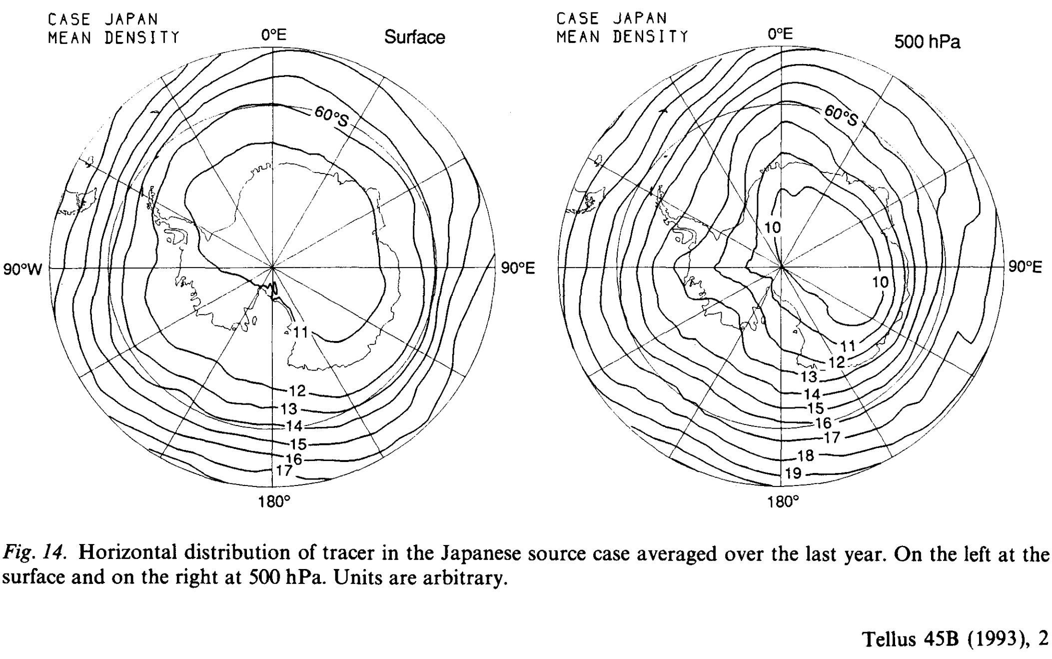

Fig. 14. Horizontal distribution of tracer in the Japanese source case averaged over the last year. On the left at the surface and on the right at 500 hPa. Units are arbitrary.

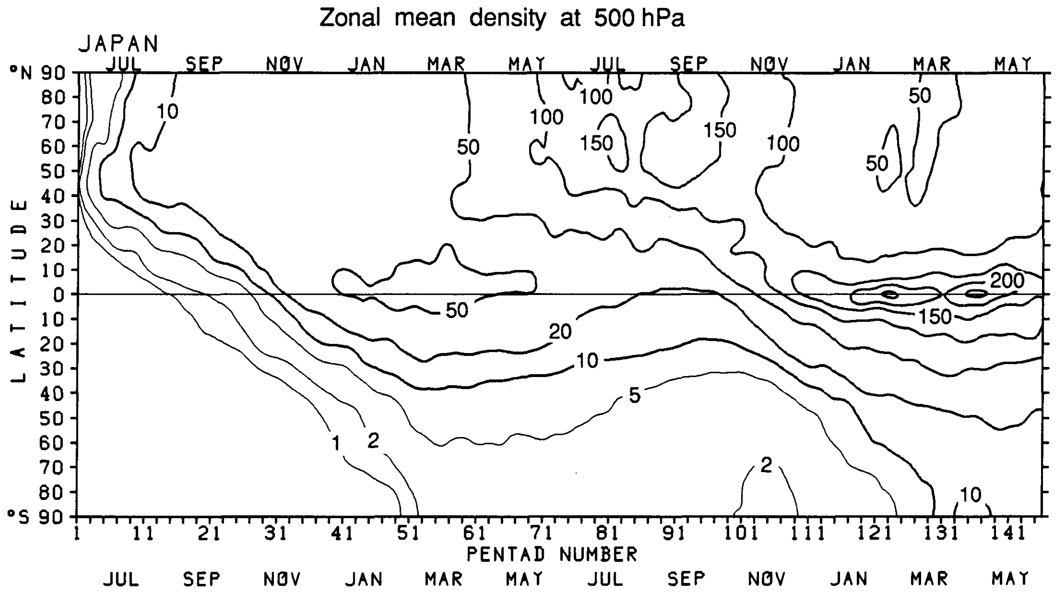

Fig. 15. Time-latitude plot of zonal mean tracer density at 500 hPa for the Japanese source case. Unit is arbitrary. Contour interval is 50. Contours of 1, 2, 5, 10, and 20 are also drawn.

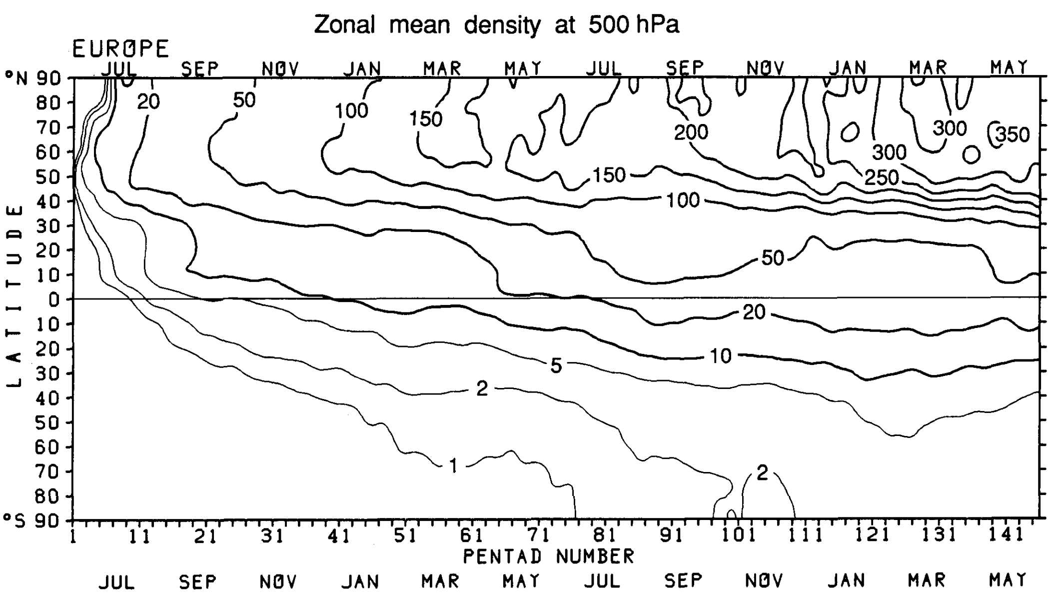

Fig. 16. Same as in Fig. 15 except for the European source case.

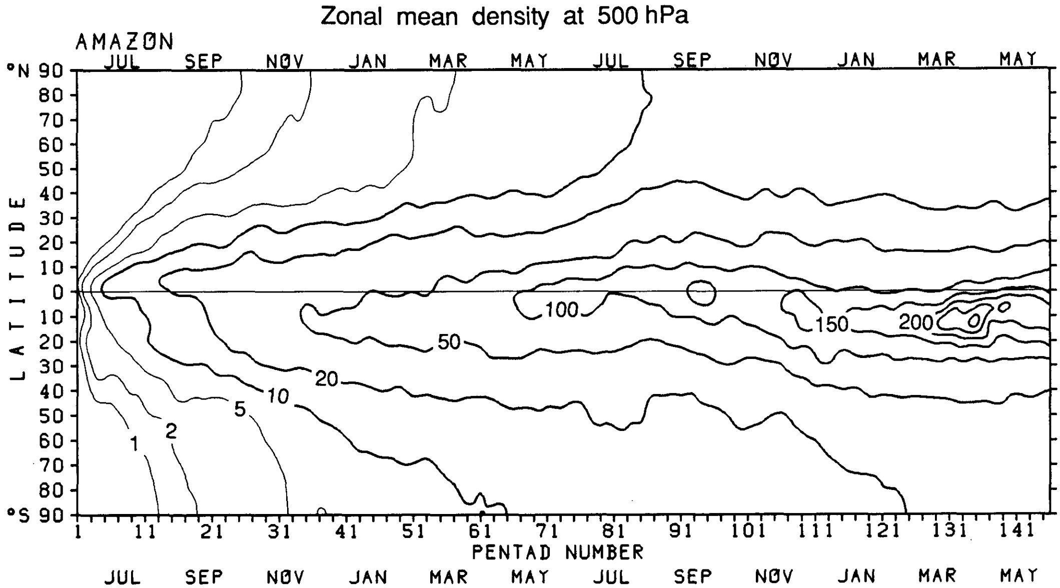

Fig. 17. Same as in Fig. 15 except for the Amazonian source case.

April of the next year (9 months later). Once tracer enters south of 40°S, the speed of meridional transport becomes fast. This fast transport is caused by baroclinic waves as shown in Fig. 3.

The temporal variation of tracer density in the southern hemisphere will be described in more detail. Fig. 18 shows line plots of the area-mean density over Antarctica (70°S ~ 90°S) and the south subtropical zone (0° ~ 31°S) for the Japanese case. Both lines exhibit clear annual variations overlapped with secular trends. The density in the south subtropical zone increases rapidly during the austral summer, while that over Antarctica lags by about 3 months. This seasonal variation in the Southern Hemisphere is solely generated by the seasonal variation of atmospheric circulation. For European and North American source cases, the temporal variations are weak and the densities are more or less monotonically increasing over Antarctica (figures not shown), though rapid increases are simulated during the austral early winter and late summer.

The observed seasonal variation of CO_2 at Antarctica and in the southern extratropics indicates a maximum in October (Tanaka et al., 1987; Nakazawa et al., 1991b), which is completely different from the Japanese source case and not similar to the other cases. Seasonal variations in the biospheric source/sink distributions are a dominant factor in determining the seasonal variation in CO_2 (Fung et al., 1983) and the seasonal variation in the atmospheric circulation appears to play a secondary role.

To examine the seasonal variations, detrended annual and semi-annual components are calculated from the last one year of the pentad data as follows. First, linear trends and averages are computed from 73 pentad time-series at each grid point. Second, a Fourier decomposition is applied to the detrended data to obtain annual and semi-annual components. Third, the components are normalized by the averages.

As mentioned before, the annual component is large for the Japanese source example. The annual component at 500 hPa for the Japanese source case is plotted in Fig. 19 with arrows. An arrow pointing northward corresponds the maximum on 9 June and time goes clockwise. The length of arrow indicates the amplitude of the anual component. The largest amplitude is found over Indonesia, where the maximum occurs in January. To the west of Indonesia over the equatorial Indian Ocean, the phase lags by about 2 months. The phase lag increases gradually on going south.

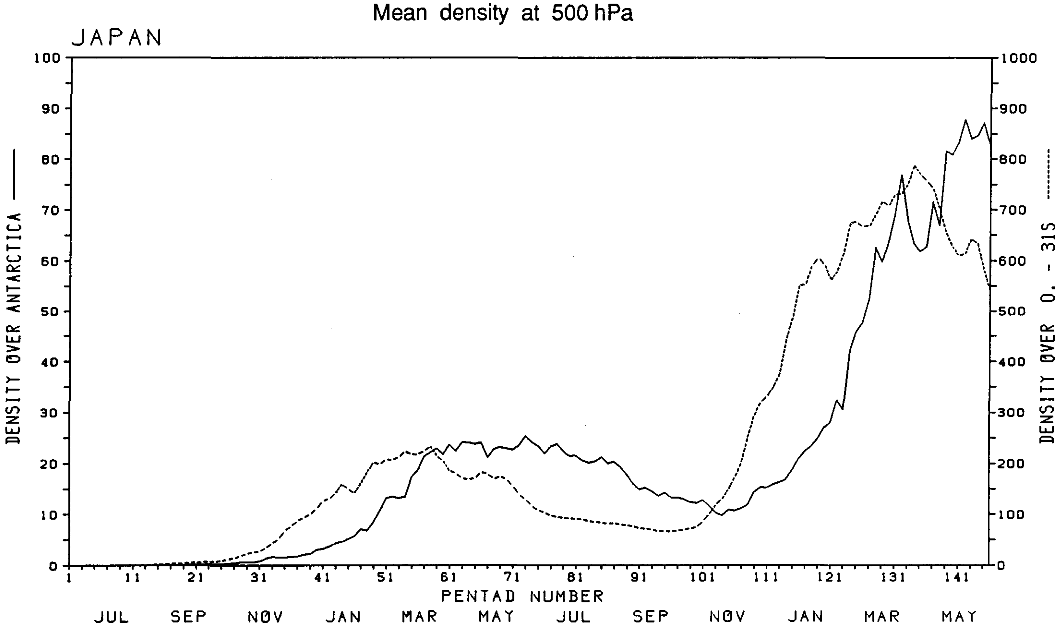

Fig. 18. Temporal variations of mean density at 500 hPa averaged over Antarctic region (solid line, the scale is on the left) and southern low-latitudes (dashed line, the scale is on the right) for the Japanese source case.

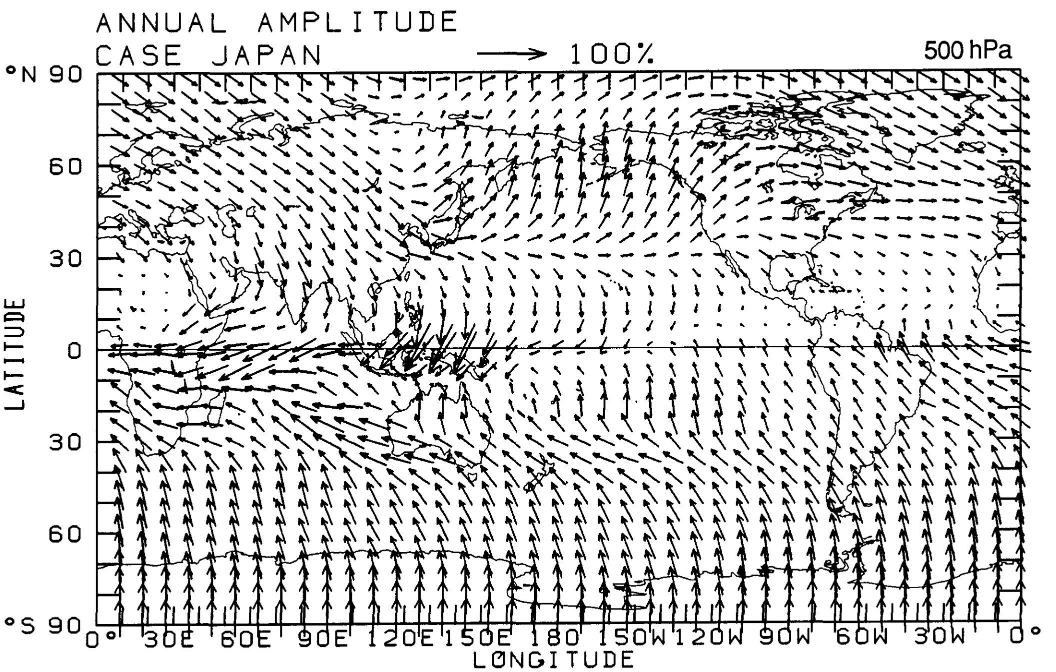

Fig. 19. Annual component of tracer density at 500 hPa for the Japanese source case (see text). The scale of the arrows is shown at the upper center of the figure. An arrow pointing upward denotes a maximum on 9 June and time goes clockwise.

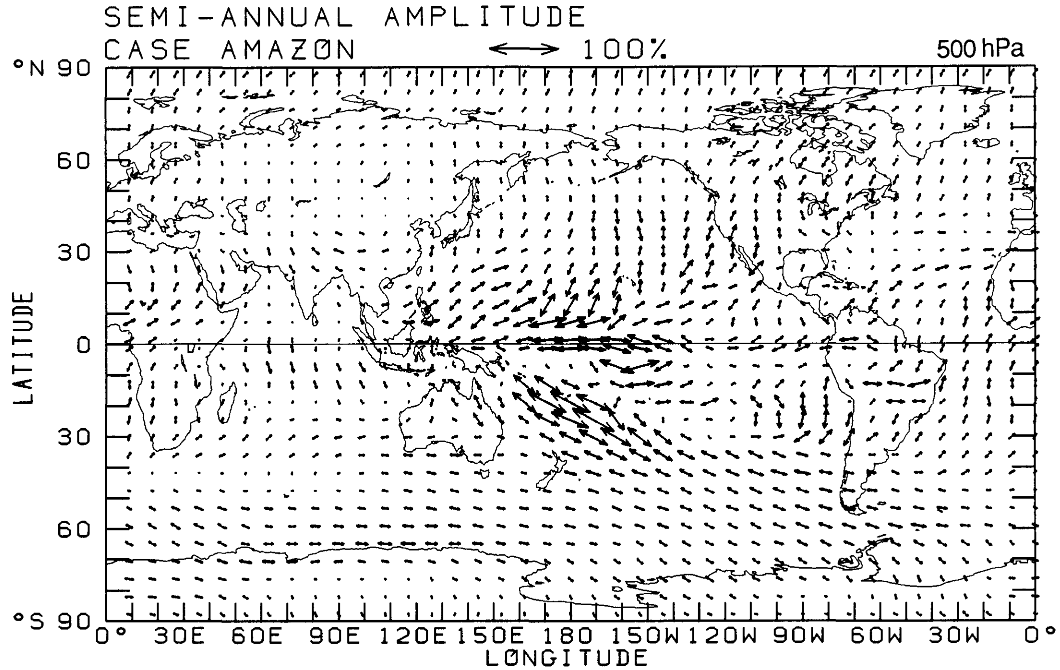

Fig. 20. Same as in Fig. 19 except for the semi-annual component of the Amazonian source case.

A relatively rapid phase change is simulated at 30–40° S. To the south of 40° S, the phase is zonally uniform and it progresses slowly toward Antarctica. Over Antarctica, the annual oscillation is as large as 60% of the mean value and the maximum occurs in early June. In the Northern Hemisphere, large amplitudes are seen over the north Pacific where the maximum occurs in June.

In the European and North American cases, both annual and semi-annual amplitudes are not large (figures not shown). In the southern extratropics, the amplitudes are larger in the upper troposphere than the middle troposphere, though the phases are coherent. This feature is common in all cases. Generally, the maximum of the annual component occurs in February and that of the semi-annual occurs in April and October in the European and North American cases.

In the Amazonian case, the annual and semi-annual components are large over the tropical Pacific. The largest amplitude of the annual component is located around 10° S, 160° W and the maximum occurs in June. In the zone of 0°–20° N over the Pacific, the magnitude of annual component is large and the maximum appears in September. In the zone of 20° S–40° S, the magnitude of the annual component is also large and the maximum appears in March. The March maximum is generally seen in the southern midlatitudes not only over the Pacific. These features are also seen in zonal mean fields (Fig. 17) and they are associated with the seasonal movement and temporal variation of the near-surface convergence regions.

The semi-annual components are as large as the annual components over the Pacific (Fig. 20). Along the equatorial Pacific, aligned arrows indicate the two maxima in March and September, which correspond to the passage of the ITCZ. Over the southwestern Pacific, there are large arrows, which are associated with the seasonal movement of the SPCZ.

5. Summary and discussion

In this study, transport simulations are performed for passive tracers emitted from Japan, Europe, North America and the Amazon regions. The transport model includes neither horizontal diffusion nor the effect of convection. Therefore, the interhemispheric exchange time simulated in this study is overestimated compared with that in the real atmosphere. Nevertheless, the qualitative conclusions derived in this study will be helpful in understanding the transport of passive tracers and in interpreting observations of anthropogenic gases.

The main results obtained are summarized here.

(i) In the case of Japanese source, an equatorward transport occurs mainly in the lower troposphere during winter associated with the Asian winter monsoon circulation. The tracer that reached the equatorial Indian Ocean is lifted and transported into the southern hemisphere. It takes about 3 months to get from the equatorial region to Antarctica, where a clear seasonal oscillation appears with the maximum in early June.

(ii) In the cases of European and North American sources, an equatorward transport is slow and a poleward transport is enhanced in winter.

(iii) In all cases, transport to the southern extratropics occurs in the upper troposphere, because the dominant upward motion advects tracers upward in the tropical region. Therefore, a vertical profile of tracer density, which increases with altitude in the troposphere, is produced in all four cases in the southern extratropics except over Antarctica.

(iv) Tracer distributions averaged over the last year in the extratropical southern hemisphere exhibit quite similar patterns in all cases, though the seasonal variations differ.

(v) There are three major transport regions in the troposphere. They are the northern/southern extratropics and tropical region. The tropical region can be divided into two subregions, i.e., the Pacific region (from Indonesia to Brazil) and the Indian Ocean region (from the Indian Ocean to Africa). Within each region, transport of tracer is fast and the distribution becomes rather uniform, whereas the transport of tracer across the border of regions takes longer time and a large gradient in tracer density is formed across the border.

(vi) In the Antarctic middle and upper troposphere, the minimum density appears over the top of East Antarctic ice sheet, whereas at the surface the distribution is rather uniform. Over the interior of the Antarctic continent, the density decreases with altitude, indicating downward transport of low-density stratospheric air.

6. Acknowledgments

The authors would like to thank K. Shibata for his contribution on developing the model. They are also grateful to anonymous reviewers for comments on the first draft. They also wish to express their appreciation to Dr. R. C. Wajsowicz for her comments on this paper. Computations were carried out on the HITAC 810/10 computer at the Meteorological Research Institute.

REFERENCES

Barrie, L. A., Olson, M. P. and Oikawa, K. K. 1989. The flux of anthropogenic sulphur into the Arctic from mid-latitudes in 1979/80. *Atmospheric Environment 23*, 2505–2512.

Chiba, M., Kida, H., Fukutani, H., Tanaka, Y., Kawahara, S., Yamada, S. and Ueno, T. 1986. A simulation of seasonal change of the atmospheric general circulation with a low resolution spectral model. Part I: Calculated monthly mean fields. *Papers in Meteorology and Geophysics 37*, 53–82.

Fung, I., Prentice, K., Matthews, E., Lerner, J. and Russell, G. 1983. Three-dimensional tracer model study of atmospheric CO_2: Response to seasonal exchange with the terrestrial biosphere. *J. Geophys. Res. 88C2*, 1281–1294.

Fung, I., Tucker, C. J. and Prentice, K. C. 1987. Application of advanced very high resolution radiometer vegetation index to study atmosphere-biosphere exchange of CO_2. *J. Geophys. Res. 92D3*, 2999–3015.

Heintzenberg, J. 1989. Arctic haze: Air pollution in polar regions. Ambio 18, 50–55.

Lacis, A. A. and Hansen, J. E. 1974. A parameterization for the absorption of solar radiation in the earth's atmosphere. *J. Atmos. Sci. 31*, 118–133.

Louis, J. F. 1979. A parametric model of vertical eddy fluxes in the atmosphere. *Boundary Layer Meteorol. 17*, 187–202.

Mahlman, J. D. and Moxim, W. J. 1978. Tracer simulation using a global general circulation model: Results from a mid-latitude instantaneous source experiment. *J. Atmos. Sci. 35*, 1340–1378.

Mahlman, J. D., Levy II, H. and Moxim, W. J. 1980.

Three-dimensional tracer structure and behavior as simulated in two ozone precursor experiments. *J. Atmos. Sci. 37*, 655–685.

Nakazawa, T., Miyashita, K., Aoki, S. and Tanaka, M. 1991a. Temporal and spatial variations of upper tropospheric and lower statospheric carbon dioxide. *Tellus 43B*, 106–117.

Nakazawa, T., Aoki, S., Murayama, S., Fukabori, M., Yamanouchi, T., Murayama, H., Shiobara, M., Hashida, G., Kawaguchi, S. and Tanaka, M. 1991b. The concentration of atmospheric carbon dioxide at the Japanese Antarctic Station, Syowa. *Tellus 43B*, 126–135.

Prather, M., McElroy, M., Wofsy, S., Russell, G. and Rind, D. 1987. Chemistry of the global troposphere: fluorocarbons as tracers of air motion. *J. Geophys. Res. 92D6*, 6579–6613.

Schlesinger, M. E. and Mintz, Y. 1979. Numerical simulation of ozone production, transport and distribution with a global atmospheric general circulation model. *J. Atmos. Sci. 36*, 1325–1361.

Shibata, K. 1989. An economical scheme for the vertical integral of atmospheric emission in longwave radiative transfer. *J. Meteorol. Soc. Japan 67*, 1047–1055.

Shibata, K. and Aoki, T. 1989. An infrared radiative scheme for the numerical models of weather and climate. *J. Geophys. Res. 94D12*, 14923–14943.

Shibata, K. and Chiba, M. 1990a. A simulation of seasonal variation of the stratospheric circulation with a general circulation model. *J. Meteorol. Soc. Japan 68*, 687–703.

Shibata, K. and Chiba, M. 1990b. Effects of radiation scheme on the surface temperature and wind over the antarctic and on circumpolar lows. *Proc. NIPR Symp. Polar Meteorol. Glaciol. 3*, 58–78.

Tanaka, T., Nakazawa, T. and Aoki, S. 1987. Seasonal and meridional variations of atmospheric carbon dioxide in the lower troposphere of the northern and southern hemispheres. *Tellus 39B*, 29–41.

Tans, P. P., Fung, I. Y. and Takahashi, T. 1990. Observational constraints on the global atmospheric CO_2 budget. *Science 247*, 1431–1438.

Williamson, D. L. and Rasch, P. 1989. Two-dimensional semi-Lagrangian transport with shape-preserving interpolation. *Mon. Wea. Rev. 117*, 102–129.

WMO 1985. Atmospheric ozone 1985. 318–337.

Yamazaki, K. and Chiba, M. 1992. Transport simulation of passive tracers from the northern hemisphere to the southern hemisphere. *Proc. NIPR Polar Meteorol. Glaciol. 5*, 9–23.